

DOI: 10.1002/ ((please add manuscript number))

Article type: Communication

A Foreign Body Response-on-a-Chip Platform

Fatemeh Sharifi[†], Su Su Htwe[†], Martina Righi[#], Hua Liu[#], Anna Peietralunga, Ozlem Yesil-Celiktas, Sushila Maharjan, Byung-Hyun Cha, Su-Ryon Shin, Mehmet Remzi Dokmeci, Nihal Engin Vrana, Amir M. Ghaemmaghammi^{}, Ali Khademhosseini^{*}, Yu Shrike Zhang^{*}*

F. Sharifi, Dr. M. Righi, Prof. H. Liu, A. Peietralunga, Prof. Dr. O. Yesil-Celiktas, Dr. S. Maharjan, Dr. B.-H. Cha, Dr. S.-R. Shin, Prof. M.R. Dokmeci, Prof. A. Khademhosseini, Dr. Y.S. Zhang^{}*

Division of Engineering in Medicine, Department of Medicine, Brigham and Women's Hospital, Harvard Medical School, Cambridge, MA 02139

E-mail: yszhang@research.bwh.harvard.edu

F. Sharifi

School of Mechanical Engineering, Sharif University of Technology, Tehran, Iran

Dr. N.E. Vrana

INSERM, UMR-S 1121, "Biomatériaux et Bioingénierie", 67085 Strasbourg, France

Protip Medical, 67000 Strasbourg, France

Université de Strasbourg, Fédération de Médecine Translationnelle de Strasbourg, Fédération des Matériaux et Nanoscience d'Alsace (FMNA), Faculté de Chirurgie Dentaire, 67000 Strasbourg, France

Dr. S.S. Htwe, Prof. A.M. Ghaemmaghammi^{}*

Immunology and Immuno-bioengineering Group, School of Life Science, Faculty of Medicine and Health Sciences, University of Nottingham, Nottingham NG7 2RD, UK

E-mail: amir.ghaemmaghami@nottingham.ac.uk

Prof. Dokmeci, Prof. A. Khademhosseini^{}*

Center for Minimally Invasive Therapeutics (C-MIT), University of California-Los Angeles, Los Angeles, CA 90095, USA

Department of Radiology, David Geffen School of Medicine, University of California-Los Angeles, Los Angeles, CA 90095, USA

Department of Bioengineering, Department of Chemical and Biomolecular Engineering, Henry Samueli School of Engineering and Applied Sciences, University of California, Los Angeles, Los Angeles, CA 90095, USA

California NanoSystems Institute (CNSI), University of California, Los Angeles, Los Angeles, CA 90095, USA

Department of Bioindustrial Technologies, Konkuk University, Seoul, Republic of Korea

E-mail: khademh@ucla.edu

[†] *Equal contribution as first authors*

[#] *Equal contribution as second authors*

Abstract

Understanding the foreign body response (FBR) and designing strategies to modulate such responses represent a grand challenge for implant devices and biomaterials. Here we report the development of a microfluidic platform, i.e., the FBR-on-a-chip (FBROC) for modeling the cascade of events during immune cell response to implants. Our platform modeled the native implant microenvironment where the implants were interfaced directly with surrounding tissues, as well as vasculature with circulating immune cells. Our study demonstrated that the release of cytokines such as monocyte chemoattractant protein 1 (MCP-1) from the extracellular matrix (ECM)-like hydrogels in the bottom tissue chamber induced the circulating monocytes in the vascular channel; resulting trans-endothelial migration of these monocytes towards the hydrogels, thus mimicking implant-induced inflammation. Data using patient-derived peripheral blood mononuclear cells further revealed inter-patient differences in such foreign body response, highlighting the potential of this platform for monitoring FBR in a personalized manner. Our prototype FBROC platform provides an enabling strategy to interrogate foreign body response on various implants, including novel biomaterials and engineered tissue constructs, in a physiologically relevant and individual-specific manner.

Keywords: foreign body response; immune response; implant, biomaterials; organ-on-a-chip

1. Introduction

Implantable devices and biomaterials have emerged as critical solutions for various healthcare problems and their use in either therapeutics or for preventive healthcare is well established [1-6]. However, adverse immune reactions against these non-self implants in the host body is often a major barrier to their success [7-12]. These adverse responses can produce dramatic negative outcomes such as excessive inflammation leading to severe tissue damage [13, 14]. Chronic inflammation on the other hand, can be detrimental for the long-term functionality of the implants eventually leading to their failure [7, 9, 10, 13].

These responses are orchestrated by different components of the immune system and in particular macrophages, have been shown to play a pivotal role in the cascade of immunological responses towards implants [15-19]. Tissue-residing macrophages and recruited immune cells (particularly neutrophils and monocytes) from the circulation are amongst the first cells that react to tissue injury as well as to the introduced foreign body including different types of implants [15, 16, 20]. One of the persistent problems around the implants, especially those that are non-degradable or slowly degradable (*e.g.*, polymeric/metallic implants), is the inability of the macrophages to resolve inflammation, provoking their tendency to maintain in the “frustrated phagocytosis” state [21]. During the beginning phase of inflammatory reactions to an injury, there is an increase of pro-inflammatory macrophages on the site, whereas a tolerogenic macrophage phenotype increases after this stage and it induces the forthcoming healing stage and allows the resolution of inflammation [17, 18, 22]. Under certain conditions such as existence of a ‘foreign body’ or some pathologies, the host immune system fails to enhance regulatory/healing macrophage levels and switch to the pro-healing stage, which ultimately leads to persistent adverse immune reactions such as the aforementioned chronic inflammation, tissue damage, fibrotic capsule formation, and dysfunction of the implant [17].

Development of strategies to properly design the implants and solutions to avoid or alleviate undesired foreign body response (FBR) represents one of the most critical challenges in

implantable medical device field. Ideally, these characterizations should be completed at an early stage of product development and pre-operative material optimizations [23]. Nevertheless, there is currently no reliable approach to determine the adverse immune responses of the human body to foreign implants prior to their *in vivo* applications. Conventional cultures of immune cells directly with these implants [24-26] do not capture the dynamic process of the FBR. Various microfluidic platforms have been recently adapted to study immunological events such as inflammation and immunotherapy [27-30], but they have rarely been used in screening the FBR to biomaterials and implants. Rodent models, including the one recently shown to recapitulate key aspects of human FBR [19], are expensive and low-throughput [31]. None of the existing approaches allow for personalized screening of the FBR to implants. Indeed, literature [32, 33] suggests a significant level of inter-individual variation that is driven by individual's immunological profile. Therefore, there is a strong need for personalized assessment of FBR at low cost and in a higher-throughput/rapid manner to select the most suitable implant material with optimal parameters, for a given patient.

Here, we report the development of a physiologically relevant **and microscopy-friendly** *in vitro* microfluidic platform, the FBR-on-a-chip (FBROC), to reproduce the dynamic effects of circulating immune cells on the implant occurring in FBR. The device consisted of a bottom tissue chamber where the implant was introduced, an endothelium to model the vasculature barrier function, and a top vascular channel to populate with circulating monocytes. The monocyte-endothelium interaction, their trans-endothelial migration, and activation against titanium (Ti) microparticles were investigated under a set of different parameters including variations on flow, endothelium, chemoattractant, and Ti implants. Proof of concept experiments using human donor-derived monocytes were further performed to reveal inter-individual differences of FBR towards Ti microparticles in our FBROC platform.

2. Results and Discussion

Organ-on-a-chip platforms have been widely used to model the dynamic processes involved in the human system *in vitro*. The combination of biomimetic cell/extracellular matrix (ECM) arrangements with microfluidic devices can be used reproduce not only the tissue microarchitecture but also the physicochemical cues under physiologically relevant conditions [34-38]. As such, the organ-on-a-chip systems are demonstrated to be superior to conventional planar, static cell culture strategies, providing improved accuracy in predicting human responses to pharmaceutical compounds, chemicals/toxins, and biological species [27, 39-42].

In this study, we have adapted this concept to study FBR in a physiologically relevant *in vitro* setting, through the development of a multi-layered FBROC system to reproduce the innate immune cell interactions with implants (**Figure 1a**). The polydimethylsiloxane (PDMS)-based FBROC system consists of a **bottom tissue chamber** where Ti microbeads were implanted as the foreign body. The **bottom tissue chamber** possessing Ti-beads was surrounded by a ring-channel containing GelMA hydrogel with or without monocyte chemoattractant protein-1 (MCP-1). The top chamber possessing an inlet and an outlet mimicked the vascular space, where immune cells (THP-1 monocytes) were allowed to circulate using a peristaltic pump. In between these two layers, a porous PET membrane was sandwiched, on top of which a monolayer of HUVECs was populated to model the endothelial barrier between the vascular lumen and the surrounding tissue. In addition, a ring-shaped PDMS spacer having the same interior window size of the underlying tissue chamber was placed below the PET membrane to provide a desired space between the endothelial layer and the bottom tissue chamber. The layers were stacked together and clamped with a pair of transparent poly(methyl methacrylate) (PMMA) plates with screw/bolt sets to ensure hydraulic tightness, similar to the setups previously reported by us and others [43, 44]. **Figure 1a** represents the schematics of different layers of the FBROC device whereas **Figure 1b** demonstrates the top and side views of the actual device.

In a typical experimental setting, the FBROC is connected to a reservoir hosting human monocytes, where the fluid flow is driven by a peristaltic pump allowing the continuous circulation of the monocytes through the top vascular chamber (**Figure 1c**). [The entire setup can be hosted in a regular cell culture incubator to ensure sufficient gas exchanges.](#) The specific dimensions of the vascular chamber are indicated in **Figure S1a**. Optimized flow conditions and monocyte distribution inside the top vascular chamber of the bioreactor was obtained using computational fluid dynamics (CFD) simulation by COMSOL Multiphysics 3.5a (Comsol Inc., Burlington, MA). Generally, fluid flow inside the microchannels are considered laminar due to the small channel dimensions and low fluid velocity ^[34]. Hence, the governing equations for obtaining flow conditions are continuity and momentum equations, *i.e.*, Eq. (1) and Eq. (2), respectively:

$$\nabla \cdot \vec{u} = 0 \quad (1)$$

$$\vec{u} \cdot \nabla \vec{u} = -\frac{1}{\rho} \nabla P + \nu \nabla^2 \vec{u} \quad (2)$$

, where \vec{u} is velocity vector and ρ , P , and ν are fluid density, pressure, and kinematic viscosity, respectively ^[45]. To obtain velocity distribution, Eq. (1) and Eq. (2) are solved simultaneously via the finite element method (FEM). RPMI used as the cell culture medium is a homogenous, Newtonian, and non-compressible fluid ^[46]. Physical properties of the fluid were considered physical properties of water at 37 °C ^[46].

Monocyte distribution was obtained by calculating trajectory of the THP-1 cells suspended throughout the culture medium by considering equation of motion for each set of particles acquired from Newton second law, hence:

$$\frac{d}{dt} (m_p \vec{u}) = \vec{F} \quad (3)$$

, where m_p is monocyte's mass and \vec{F} is total force experienced by them. The total force exerted on the monocytes were composed of three components: drag force, Brownian and gravity. Therefore, the total force in the equation of motion can be written as:

$$\frac{d\mathbf{u}_p}{dt} = F_D + g \left(\mathbf{1} - \frac{\rho}{\rho_p} \right) \quad (4)$$

, where \mathbf{u}_p denotes particle velocity, F_D is drag force, g is the gravity acceleration, and ρ_p is the monocytes density. Drag force is obtained as:

$$F_D = 3\pi\mu\mathbf{u}_{rel}d_p \quad (5)$$

, where μ indicates fluid viscosity, $\mathbf{u}_{rel} = \mathbf{u}_{fluid} - \mathbf{u}_p$, and d_p is monocyte diameter. For obtaining monocyte distribution, it was assumed that the impact of the cell motion on the fluid flow was negligible ^[47]. Therefore, first-velocity field was estimated and hence, monocyte trajectories were computed.

The optimal inlet velocity was obtained by taking into consideration of factors including shear stress imposed on both monocytes and HUVECs, velocity profile inside the channel, the distribution of the circulating monocytes, and the duration for the monocytes to interact and pass through the endothelium barrier. Average shear stress sensed by the vascular endothelial cells in the human body is between 5-10 dyne cm⁻² ^[48]. It is widely acknowledged that hemodynamic forces have a great impact on endothelial cells and are critical for normal vessel wall functionalities. For example, shear stress changes the shape and orientation of the endothelial cells in culture; cells might not align in the direction of the flow under low shear stress conditions while elevated shear stress is detrimental to the cells ^[49]. On the other hand, shear stress also affects the monocyte-endothelium interactions. Monocyte rolling and arrest to the endothelium are influenced by both force and contact time applied to them ^[46, 50], where shear rate of 400 s⁻¹ (translating to ~3.6 dyne cm⁻² in biological medium with a viscosity of 8.9×10⁻⁴ Pa-s, see **Table 1**) is considered as a threshold for monocyte adhesion ^[49].

Streamline distribution of the medium flow inside the vascular channel is shown in **Figure S1b**, suggesting that the flow was largely laminar. Simulation of monocyte distribution inside the entire vascular chamber with a density of 1 × 10⁶ cells mL⁻¹ at the optimized flow rate of 400 μL min⁻¹, in perspective and cross-sectional/front views, are depicted in **Figure 2a and 2b**,

respectively, indicating that the cells could be uniformly distributed across the chamber emulating their homogeneous distributing profiles in circulation in blood vessels in the human system.

To create the functional endothelial barrier between the vascular chamber and the tissue chamber, HUVECs were seed on the surface of the PET membrane (3 μm in pore size) at a density of 7.5×10^4 cells cm^{-2} . The formation of a continuous monolayer of HUVECs was observed after 72 h under static culture conditions. Similarly, when the HUVECs were cultured under dynamic condition at the flow rate of $400 \mu\text{L min}^{-1}$ for the same period, the continuous monolayer of HUVECs was formed, consistent with our previous observations^[43] and literature^[51]. The phenotype of the endothelial monolayer on the PET porous membrane was further characterized by immunostaining of HUVECs with endothelial biomarkers such as vascular endothelial (VE)-cadherin and intercellular adhesion molecule 1 (ICAM1). VE-cadherin^[52] and ICAM1^[53] are endothelial-specific adhesion molecules that are consistently expressed on the membranes of and at junctions between endothelial cells. Fluorescence microscopy images of the immunostained endothelial monolayer formed on the PET porous membrane exhibited strong expression of VE-cadherin and ICAM1 under both static (**Figure 2c and d**, respectively) and dynamic (**Figure 2e and f**, respectively) conditions, indicating that the flow rate used did not have adverse effects on the function of the endothelial cells.

The endothelialized porous PET membrane was subsequently integrated into the FBROC platform to evaluate the monocyte-endothelium interactions. Human THP-1 monocytes were suspended in a 50:50 monocyte culture medium (RPMI 1640) and endothelial growth medium (EGM-1). We compared the expressions of CD80, a class of co-stimulatory receptors, on the monocytes under static and dynamic conditions using CD80 antibody. It has been shown that the freshly isolated monocytes do not express CD80 and CD80 expression is enhanced by stimulation in *in vitro* cultures^[54]. Immunostaining of THP-1 monocytes with CD80 antibody and fluorescence microscopy analyses performed after 4 days of dynamic culture revealed the

expression of CD80 (**Figure 2g-j**), suggesting the activation and interaction of THP-1 monocytes with the HUVECs through attachment and spreading on the endothelial barrier under fluid flow, possibly induced by shear stress and the rolling effect ^[55-57]. On the contrary, under static culture condition (*i.e.*, no fluid flow) expression of CD80 by THP-1 minimum amount of monocytes was observed on the endothelial barrier indicating that the TPH-1 cells became barely activated with limited interactions of these cells with the endothelium (**Figure 2k-o**). These results demonstrated the importance of creating a dynamic *in vivo*-mimetic condition since dynamic flow seems to be critical in reproducing the interactions between immune cells and endothelium, as widely reported ^[55-57].

We next analyzed the migration of THP-1 monocytes through the endothelial barrier. Specifically, compared the monocyte migration under static and dynamic conditions, as well as in the absence and presence of monocyte chemoattractant protein 1 (MCP-1). MCP-1 is a key chemokine regulating the migration/infiltration of immune cells such as monocytes and macrophages, and is released by the stromal tissues upon implantation of foreign materials during FBR ^[58]. To mimic such a process, we encapsulated MCP-1 in a ring of gelatin methacryloyl (GelMA) hydrogel at the bottom chamber of the device, surrounding the tissue chamber coated with Ti microbeads (**Figure 3a**). GelMA hydrogel is a porous and biocompatible material that has been used extensively in tissue engineering because it closely resembles some of the essential properties of the native ECM including inherent bioactivity and broadly tunable physicochemical behaviors ^[59, 60]. The release of MCP-1 from the GelMA ring was quantified by collecting the medium outflow from the top vascular chamber under the same perfusion condition in the presence of the endothelial barrier, which showed a sustained release profile over the 4-day period with an initial burst release in the first day (**Figure 3b**).

When THP-1 monocytes pre-labeled with cell tracker red were cultured on the vascular channel on the top of the PET membrane with HUVECs-monolayer under the static condition and in the absence of MCP-1, only very few cells could transmigrate through the endothelium

to reach Ti microbeads at the bottom chamber at day 4 (**Fig. 3c**). Whereas, increased number of THP-1 monocytes were found to have transmigrated through the endothelium when MCP-1 was slowly released from the GelMA ring for the same period of time (**Fig. 3d**). However, under the dynamic flow condition the transendothelial migration of THP-1 monocytes was significantly higher both in the presence and absence of MCP-1 when compared to those under static conditions (**Figure 3e and 3f**). The quantitative analyses of migration of THP-1 monocytes through the endothelial barrier under different conditions have been shown in **Figure 3g**. These results were consistent with our monocyte activation results (**Figure 2i-p**), where flow was found to be an important parameter.

The differentiation of THP-1 monocytes into M1 or M2 phenotypes was subsequently evaluated by immunostaining of the cells with CD80 or CD206 antibodies, respectively, after they have migrated through the endothelial barrier and attached onto the Ti microbeads, under dynamic flow condition at day 4. CD80 is M1-specific phenotype marker and thus overexpressed in pro-inflammatory (M1) subtype cell population whereas CD206 is M2 phenotype marker whose expression is increased as the cells differentiate into anti-inflammatory alternatively activated (M2) subtype cell population [61, 62]. Immunofluorescence studies revealed that the increased number of transendothelial migrated THP-1 cells were differentiated into CD80-positive cells, primarily located in the tissue chamber containing Ti microbeads, both in the absence (**Figure 3h**) and presence (**Figure 3i**) of MCP-1 indicating that the differentiation of THP-1 was almost entirely towards the pro-inflammatory M1 phenotype and thus confirming the recognition of the Ti microbeads as foreign body by the THP-1 cells. As expected, the number of monocytes migrated across the endothelial barrier and attached to the Ti microbeads was higher when MCP-1 was released. Cytokine quantification at Day 4 under dynamic culture in the presence of MCP-1 further revealed the overwhelming secretion of the pro-inflammatory cytokine interleukin (IL)-6 reaching a value of $403 \pm 46.5 \text{ pg mL}^{-1}$, where its baseline concentration in standard THP-1 monocyte culture has been well-shown to

be minimum ^[63]. This observation was consistent with the immunostaining results and the fact that IL-6 is a pro-inflammatory cytokine that is linked to pro-inflammatory responses by monocytes ^[64].

We finally extended our FBROC platform for studying human primary immune cell responses to implants. Instead of the human THP-1 monocyte cell line, we isolated primary human monocytes from donor-derived peripheral blood mononuclear cells (PBMCs), and perfused these cells in the top vascular chamber of the FBROC device, containing the same Ti microbeads in the bottom tissue chamber. The presence of the endothelium and the dynamic flow seemed to be essential in activating the interactions of the human primary monocytes with the barrier as shown by CD206 staining on monocytes and VE-cadherin staining on HUVECs (**Figure 4a**). Similar to the results obtained with THP-1 cell line, the release of MCP-1 from the bottom tissue chamber had a positive effect on inducing the trans-endothelial migration of the human primary monocytes, as shown in both nuclei staining (**Figure 4b**) and in quantification analyses (**Figure 4c**).

Similarly, the M1/M2 differentiation of the human primary monocytes was also analyzed and found that for the specific donor shown in **Figure S2**, in either absence or presence of Ti microbeads in the bottom tissue chamber of the bioreactor the primary monocytes expressed both M1- and M2-associated surface markers approximately in equal ratio, with most cells exhibiting double stains. The differences of M1/M2 differentiation in response to the Ti microbeads between the human primary monocytes and the THP-1 monocytes could possibly be explained by the fact that, in the cell line the expression of each marker is induced in response to different environmental stimuli, while in the primary cells these markers are constitutively expressed and the intensities of expressions change when responding to different stimuli ^[64-68]. Indeed, when we examined the FBR of the monocytes derived from three different donors, it was found that, interestingly, different individuals exhibited varying degrees of immune responses to the same Ti microbeads (**Figure 4d**). While two donors (Donor B and Donor C)

did not exhibit noticeable difference in M1/M2 differentiation of their PBMC-derived monocytes, one donor (Donar A) had strong pro-inflammatory reaction to the Ti microbeads (**Figure 4e,f**), clearly indicating that there is likely a ‘population spectrum’ of responses to the same implant possibly due to differences in receptor expressions and cytokine profiles of the immune cells [32, 33]. It should be noted that, this dataset achieved with human primary monocytes from healthy donors was different from that observed when human THP-1 monocyte cell line was used (which always showed pro-inflammatory phenotype). This fact further confirmed that the FBR is closely dependent on the specific populations of immune cells that confer variations in their reactions to foreign implants, which can be effectively tested on our FBROC platform.

3. Conclusions

In summary, we have reported the design and fabrication of multi-layered FBROC system to mimic the immune cell-foreign body interactions *in vitro* using THP-1 monocyte cells circulating through the topmost vascular channel, separated from the bottom tissue chamber, containing Ti microbeads as the foreign body material, by a PET porous membrane coated with a monolayer of HUVECs. The addition of MCP-1 in the GelMA hydrogel, that functions as ECM surrounding the Ti microbeads, stimulated the monocyte-endothelial cell interactions and transendothelial migration of THP-1 cells as demonstrated by the immunostaining of cell specific biomarkers. Similarly, we have observed that most of the transmigrated THP-1 cells differentiated into the pro-inflammatory M1 phenotype, and thus confirming the recognition of the Ti microbeads as foreign body by the THP-1 cells. In contrast to the THP-1 cell line, differentiation of primary human monocytes into M1 and M2 phenotypes vary from one donor to other, thus indicating the importance of personalized FBROC system to study the inter-patient difference in foreign body response. Once the FBR is screened on the FBROC platform, methods of immunomodulation [69-72] may then be accordingly personalized to mitigate the

negative immune responses of the host towards the foreign body. Thus, we believe that the FBROC system has a potential to expand the studies of personalized FBR on vast categories of subjects including but not limited to, implants reported in the current work as well as biologically active materials and engineered tissues.

4. Experimental Section

Materials

Sylgard[®] 184 Silicone Elastomer kit was purchased from Dow Corning Corporation (Midland, MI, USA) and PMMA sheets were obtained from McMaster-Carr (Elmhurst, IL, USA) and Goodfellow (Coraopolis, PA, USA). Gelatin from porcine skin (type-A, 300 bloom), methacrylic anhydride, 2-hydroxy-4'-(2-hydroxyethoxy)-2-methylpropiophenone (photoinitiator, PI, Irgacure 2959), triton X-100, and bovine serum albumin (BSA) were purchased from Sigma-Aldrich (St. Louis, MO, USA). Dulbecco's phosphate-buffered saline (DPBS), fetal bovine serum (FBS), trypsin-ethylenediaminetetraacetic acid (trypsin-EDTA), penicillin/streptomycin, 4',6-diamidino-2-phenylindole (DAPI), Live/Dead[®] Viability Kit, PrestoBlue[®] Cell Viability Reagent, RPMI 1640 medium, and PET cell culture inserts were purchased from ThermoFisher Scientific (Waltham, MA, USA), whereas endothelial growth medium-2 (EGM-2) was obtained from Lonza (Walkersville, MD, USA). Medical-grade (Grade 2, Neyco) Ti microbeads were supplied by PROTiP Medical (Strasbourg, France). Primary antibodies against human VE-cadherin, ICAM-1, CD80, and CD206, as well as Alexa Fluor[®] 594- and Alexa Fluor[®] 555-conjugated secondary antibodies were purchased from Abcam (Cambridge, MA, USA). Mouse anti-human CD31 primary antibody was purchased from Dako (Santa Clara, CA, USA). Recombinant human CCL2/JE/MCP-1 and all enzyme-linked immunosorbent assay (ELISA) kits were obtained from R&D Systems (Minneapolis, MN, USA). All other chemicals used in this study were obtained from Sigma-Aldrich unless otherwise noted.

Synthesis of GelMA

GelMA was synthesized according to our previously published protocol [73-75], at a high degree of methacryloyl substitution ($81.4 \pm 0.4\%$). Briefly, 10 g of type A gelatin from porcine skin was dissolved in 100 mL of DPBS at 60 °C using magnetic stirrer and 8.0 mL of methacrylic anhydride was added drop wisely to the gelatin solution under continuous stirring condition. The reaction was carried out for 3 h at 50 °C and then quenched by a 5-fold dilution of the reaction mixture with warm DPBS (40 °C). The product obtained was dialyzed against distilled water at 40 °C for 7 days using 12–14 kDa cutoff dialysis tubing to remove unreacted methacrylic anhydride. GelMA solution was finally lyophilized and stored at room temperature until further use.

Cell Culture

HUVECs expressing green fluorescent protein (GFP) purchased from Angio-Proteomie (Boston, MA, USA) were cultured in EGM-2 while human monocytes (THP-1) obtained from ATCC (Manassas, VA, USA) were cultured in RPMI 1640 medium supplemented with 10 % (v/v) FBS and 1% (v/v) penicillin-streptomycin. The cell cultures were maintained at 37 °C and 5% CO₂ in a standard incubator. The medium was replaced every 2–3 days and the cells cultured in flasks were subcultured when they reached approximately 80% confluency. For on-chip experiments, we used a 1:1 volume mixture of the two media as the common medium, which we did not observe any adverse effects on either cell type.

Fabrication of the FBROC device

The FBROC device consisting of four layers was designed and fabricated as shown in **Figure 1**. Each layer of the chip was designed using CorelDraw (Corel Corp, Ottawa, ON) and imported to a laser cutting system (VLS 2.30 Desktop Laser, Universal Laser Systems Inc,

Richmond, VA) for cutting PMMA sheets (3 mm or 1.6 mm in thickness) into desired sizes and patterns to serve as the molds. PDMS precursor prepared by mixing the monomer and curing agent at the ratio of 10:1, was then poured onto the PMMA molds, cured at 85 °C for 2 h, and peeled off. The top layer consisted the vascular channel for circulating immune cells and the bottom layer consisted the tissue chamber coated with titanium beads ($d=150\ \mu\text{m}$). In between these two layers, a porous PET membrane of 3 μm in pore size was sandwiched, on top of which a monolayer of endothelial cells was populated to model the endothelial barrier between the vascular lumen and the surrounding tissue. In addition, a ring-shaped PDMS spacer having the same internal window size of the underlying tissue chamber was placed below the PET membrane. All these layers were held together tightly using a pair of PMMA (3 mm in thickness) clamped with sets of screws and bolts. The microfluidic chamber on top, composed of an inlet and an outlet, was connected to a peristaltic pump using turbo tubings thus allowing the circulation of THP-1 cells.

Fluid dynamics modeling and simulation

The flow velocity and shear stress profiles in the FBROC device were investigated with 3D CFD simulation using FEM implemented in COMSOL Multiphysics 3.5a (Comsol Inc., Burlington, MA). Equations of continuity (Eq. 1) and momentum (Eq. 2) were solved simultaneously to obtain fluid velocity distribution. Monocyte distribution was obtained by considering equation of motions and calculating three forces (*i.e.*, drag, Brownian, and gravity) imposed on the cells *via* the Lagrangian method. Constants used for the simulation are provided in **Table 1**.

Table 1. Parameters and constants used for modeling.

Simulation parameter: Symbol [SI unit]	Value
--	-------

Density of the fluid: ρ [kg/m ³]	1000 [46]
Viscosity of the fluid: μ [Pa-s]	8.9×10^{-4} [46]
Density of the monocytes: ρ_p [kg/m ³]	1077 [76]
Diameter of the monocytes: d_p [μ m]	15 [77]

Morphological observations

To observe the morphology of GFP-HUVECs in the FBROC device, after 4 days of dynamic experiment, the device was disassembled and the GFP-HUVECs on the PET membrane were fixed with 4% (v/v) paraformaldehyde for 20 min. The cells were permeabilized with 0.1% (v/v) Triton X-100 in DPBS for 30 min and then blocked with 1% (w/v) BSA in DPBS, followed by F-actin staining by incubating the cells with Alexa Fluor[®] 594-phalloidin (1:40 dilution in 0.1% (w/v) BSA) for 1 h at room temperature. After washing with DPBS, nuclei were counter-stained with DAPI for 5 min at room temperature. Finally, the cells were observed using AxioObserver D1 inverted fluorescence microscope (Zeiss, Thornwood, NY, USA).

Attraction of circulating monocytes

MCP-1 was used as a chemoattractant to attract monocytes towards the bottom tissue chamber containing the Ti microbeads, simulating the cytokine released by the local tissue in response to the foreign body material. In both static and dynamic experiments, 50 ng mL⁻¹ of MCP-1 was encapsulated in the 5 w/v% GelMA hydrogel containing 0.5% w/v PI. The GelMA hydrogel with MCP-1 was poured into ring-shaped channel surrounding the Ti microbeads in the bottom tissue chamber and then crosslinked by exposing under UV light (800 mW cm⁻²) for 30 s.

Transendothelial migration of monocytes through HUVEC monolayers under flow

Migration of monocytes through the endothelium was monitored by labeling with cell tracker (CM Dil dye, Thermo Fisher, Waltham, MA, USA). The cells suspended in the medium was first harvested by centrifuging at 200g for 5 min. Harvested cells were mixed with CM Dil dye solution at the concentration of 1 $\mu\text{L mL}^{-1}$ in DPBS and incubated at 37 °C for 5 min and then at 4 °C for 15 min. The monocytes were then suspended in the medium after washing with DPBS for further use. During dynamic experiments, these CM Dil-stained monocytes were allowed to circulate continuously through the upper vascular channel within the FBROC device. The THP-1 cells transmigrated across the endothelium and accumulated in the tissue chamber were observed using the fluorescence microscope.

Human primary monocytes

Buffy coats from healthy donors were obtained from the National Blood Service (National Blood Service, Sheffield, UK) following ethics committee approval (2009/D055). PBMCs were isolated by Histopaque-1077 (Sigma-Aldrich) density gradient centrifugation. Monocytes were isolated from PBMCs by positive selection of CD14⁺ cells using the MACS magnetic cell separation system (Miltenyi Biotec) as described before [78, 79]. This method routinely yielded >95% pure monocytes as determined by flow cytometric analysis of CD14 expression. All methods were performed in accordance with the relevant guidelines and regulations.

ELISA

All reagents were brought to the room temperature before starting the assay. A 200- μL volume of standard or sample was added to each monoclonal MCP-1-specific antibody-precoated 96 microplate well and incubated for 2 h at room temperature. Then each well was aspirated and washed three times with washing buffer. Next, a 200- μL volume of MCP-1 conjugate (polyclonal antibody specific for human MCP-1 conjugate) was added to each well and incubated 1 h at room temperature, which was then followed by three washes. Stabilized

hydrogen peroxide and stabilized chromogen (tetramethylbenzidine) were mixed within 15 min of use in equal volumes to reconstitute the substrate solution. A 200- μ L volume of this solution was added to each well and incubated for 30 min at room temperature protected from light. Finally, 50 μ L of 2N sulfuric acid as the stop solution was added to each well. The optical density of each well was determined by a microplate reader (BioTek, VT, US) at 450 nm with 540 nm as wavelength correction. Samples were run in triplicates unless otherwise stated.

Immunocytochemical analyses

To demonstrate the functions of HUVECs, the cells on the PET membrane were immunostained for VE-cadherin, CD31, and ICAM-1. At designated time points, HUVECs on the PET membrane were washed with DPBS and fixed with 4% (w/v) paraformaldehyde for 20 min, followed by incubation with permeabilization buffer (0.1% (v/v) Triton X-100 in DPBS) for 30 min at room temperature. The cells were blocked with 1% (w/v) BSA in DPBS for 1 h at room temperature and incubated overnight with the primary antibody (1:200 dilution) at 4 °C. After washing with DPBS, the samples were incubated with the secondary antibody at 1: 200 dilution (Alexa Fluor[®] 555-conjugated goat anti-rabbit for VE-cadherin and Alexa Fluor[®] 594-conjugated goat anti-mouse for CD31 or ICAM-1) for 1 h at room temperature. After washing with DPBS, nuclei were counter-stained with DAPI and then examined under fluorescence microscope. Similarly, the differentiation of THP-1 monocytes or human primary monocytes into M1 or M2 phenotypes was evaluated by immunostaining of the cells with CD80 (1:80 dilution) and CD206 (1:100 dilution) antibodies. For quantifying the expression ratios of CD80/CD206 on primary monocytes, mean fluorescence intensities of the respective channels were calculated using ImageJ.

Statistical analysis

Sample sizes were 3 in all cases. Data were presented as mean \pm standard deviations. Statistical analysis was performed using unpaired t-tests. The statistical significance was determined with $p < 0.05$ and $p < 0.01$.

Supporting Information

Supporting Information is available from the Wiley Online Library or from the author.

Acknowledgments

The authors acknowledge funding from the National Institutes of Health (AR057837, DE021468, D005865, AR068258, AR066193, EB022403, EB021148) and the Presidential Early Career Award for Scientists and Engineers (PECASE) and the Fundamental Research Funds for the Central Universities from China (No. 14D310106). Y.S.Z. acknowledges funds from the National Institutes of Health (K99CA201603, R21EB026175, R21EB026175) and the New England Anti-Vivisection Society (NEAVS). This project further received funding from the European Union's FP7 and Horizon 2020 research and innovation programme under grant agreement No. 602694 (IMMODGEL) and No. 760921 (PANBioRA) (N.E.V., A.M.G., A.K.).

Received: ((will be filled in by the editorial staff))

Revised: ((will be filled in by the editorial staff))

Published online: ((will be filled in by the editorial staff))

References

- [1] K. Fukumitsu, H. Yagi, A. Soto-Gutierrez, "Bioengineering in organ transplantation: targeting the liver", 2011.
- [2] R. Langer, J. P. Vacanti, *Science* 1993, 260, 920.
- [3] S. Rafii, D. Lyden, *Nat. Med.* 2003, 9, 702.
- [4] M. Breitbart, T. Bostani, W. Roell, Y. Xia, O. Dewald, J. M. Nygren, J. W. Fries, K. Tiemann, H. Bohlen, J. Hescheler, A. Welz, W. Bloch, S. E. Jacobsen, B. K. Fleischmann, *Blood* 2007, 110, 1362.
- [5] A. Nakamura, M. Akahane, H. Shigematsu, M. Tadokoro, Y. Morita, H. Ohgushi, Y. Dohi, T. Imamura, Y. Tanaka, *Bone* 2010, 46, 418.
- [6] M. Fernández-Ruiz, D. Kumar, A. Humar, *Clinical & translational immunology* 2014, 3, e12.
- [7] S. F. Badylak, T. W. Gilbert, "Immune response to biologic scaffold materials", 2008, 2008.
- [8] P. N. Martins, J. Pratschke, A. Pascher, L. Fritsche, U. Frei, P. Neuhaus, S. G. Tullius, *Transplantation* 2005, 79, 127.
- [9] J. M. Anderson, *Problems in General Surgery* 1994, 11, 147.
- [10] J. M. Anderson, A. Rodriguez, D. T. Chang, "Foreign body reaction to biomaterials", 2008, 2008.
- [11] W. K. Ward, SAGE Publications, 2008.
- [12] D. F. Williams, *Biomaterials* 2008, 29, 2941.
- [13] J. Anderson, S. Cramer, *Host Response to Biomaterials: The Impact of Host Response on Biomaterial Selection* 2015, 13.
- [14] A. Remes, D. F. Williams, *Biomaterials* 1992, 13, 731.
- [15] J. M. Anderson, K. Defife, A. McNally, *J. Mater. Sci. Mater. Med.* 1999, 10, 579.
- [16] Z. Xia, J. T. Triffitt, *Biomed. Mater.* 2006, 1, R1.
- [17] S. F. Badylak, J. E. Valentin, A. K. Ravindra, G. P. McCabe, A. M. Stewart-Akers, *Tissue Eng. A* 2008, 14, 1835.
- [18] M. Scatena, K. V. Eaton, M. F. Jackson, S. A. Lund, C. M. Giachelli, in *The Immune Response to Implanted Materials and Devices*, Springer, 2017, 37.
- [19] J. C. Doloff, O. Veiseh, A. J. Vegas, H. H. Tam, S. Farah, M. Ma, J. Li, A. Bader, A. Chiu, A. Sadraei, *Nat. Mater* 2017, 16, 671.
- [20] J. M. Anderson, S. Jiang, in *The Immune Response to Implanted Materials and Devices*, Springer, 2017, 15.
- [21] R. Klopffleisch, F. Jung, *J. Biomed. Mater. Res. A* 2017.
- [22] J. Kzhyshkowska, A. Gudima, V. Riabov, C. Dollinger, P. Lavalle, N. E. Vrana, *J. Leukocyte Biol.* 2015, 98, 953.
- [23] D. Williams, *J. Biomed. Eng.* 1989, 11, 185.
- [24] M. J. Smith, K. L. White, D. C. Smith, G. L. Bowlin, *Biomaterials* 2009, 30, 149.
- [25] B. Panilaitis, G. H. Altman, J. Chen, H.-J. Jin, V. Karageorgiou, D. L. Kaplan, *Biomaterials* 2003, 24, 3079.
- [26] M. Feito, M. Vila, M. Matesanz, J. Linares, G. Gonçalves, P. Marques, M. Vallet-Regí, J. Rojo, M. Portolés, *J. Colloid Interface Sci.* 2014, 432, 221.
- [27] E. Biselli, E. Agliari, A. Barra, F. R. Bertani, A. Gerardino, A. De Ninno, A. Mencattini, D. Di Giuseppe, F. Mattei, G. Schiavoni, *Sci. Rep.* 2017, 7, 12737.
- [28] D. Irimia, X. Wang, *Trends Biotechnol.* 2018.
- [29] N. Moore, D. Doty, M. Zielstorff, I. Kariv, L. Moy, A. Gimbel, J. Chevillet, N. Lowry, J. Santos, V. Mott, *Lab Chip* 2018.
- [30] J. M. Heintze, *Nature Reviews Nephrology* 2018, 14, 354.
- [31] J. Mestas, C. C. W. Hughes, *The Journal of Immunology* 2004, 172, 2731.

- [32] K. Buscher, E. Ehinger, P. Gupta, A. B. Pramod, D. Wolf, G. Tweet, C. Pan, C. D. Mills, A. J. Lusic, K. Ley, *Nature Communications* 2017, 8, 16041.
- [33] P. Martín-Fuentes, F. Civeira, D. Recalde, A. L. García-Otín, E. Jarauta, I. Marzo, A. Cenarro, *The Journal of Immunology* 2007, 179, 3242.
- [34] D. Huh, G. A. Hamilton, D. E. Ingber, *Trends Cell Biol.* 2011, 21, 745.
- [35] C. Moraes, G. Mehta, S. C. Leshner-Perez, S. Takayama, *Ann. Biomed. Eng.* 2012, 40, 1211.
- [36] S. N. Bhatia, D. E. Ingber, *Nat. Biotechnol.* 2014, 32, 760.
- [37] K. Yum, S. G. Hong, K. E. Healy, L. P. Lee, *Biotechnology journal* 2014, 9, 16.
- [38] F. Zheng, F. Fu, Y. Cheng, C. Wang, Y. Zhao, Z. Gu, *Small* 2016, n/a.
- [39] E. W. Esch, A. Bahinski, D. Huh, *Nature Reviews Drug Discovery* 2015, 14, 248.
- [40] A. Skardal, T. Shupe, A. Atala, *Drug Discov. Today* 2016, 21, 1399.
- [41] Y. Li, K. Zhu, X. Liu, Y. S. Zhang, *Curr. Drug Metab.* 2018, 19, 100.
- [42] Y. S. Zhang, Y.-N. Zhang, W. Zhang, *Drug Discov. Today* 2017, 22, 1392.
- [43] Y. S. Zhang, J. Aleman, S. R. Shin, T. Kilic, D. Kim, S. a. M. Shaegh, S. Massa, R. Riahi, S.-K. Chae, N. Hu, H. Avci, W. Zhang, A. Silvestri, A. Manbohi, A. Polini, G. Calzone, N. Shaikh, A. Sanati, P. Alerasool, N. S. Bhise, E. Budina, A. Pourmand, A. Skardal, T. Shupe, C. Bishop, M. R. Dokmeci, A. Atala, A. Khademhosseini, *Proceedings of the National Academy of Sciences USA* 2017, 114, E2293.
- [44] A. Skardal, S. V. Murphy, M. Devarasetty, I. Mead, H.-W. Kang, Y.-J. Seol, Y. S. Zhang, S.-R. Shin, L. Zhao, J. Aleman, A. Hall, T. Shupe, A. Kleensangb, M. R. Dokmeci, S. J. Lee, J. Jackson, J. Yoo, T. Hartung, A. Khademhosseini, S. Soker, C. Bishop, A. Atala, *Sci. Rep.* 2017, 7, 8837.
- [45] F. M. White, I. Corfield, *Viscous fluid flow*, Vol. 3, McGraw-Hill New York, 2006.
- [46] K. D. Rinker, V. Prabhakar, G. A. Truskey, *Biophys. J.* 2001, 80, 1722.
- [47] W. B. Russel, D. A. Saville, W. R. Schowalter, Press, Cambridge 1989.
- [48] C. F. Dewey, S. R. Bussolari, M. A. Gimbrone, P. F. Davies, *J. Biomech. Eng.* 1981, 103, 177.
- [49] M. Grigioni, C. Daniele, G. D'avenio, V. Barbaro, *J. Biomech.* 1999, 32, 1107.
- [50] G. Theilmeier, T. Lenaerts, C. Remacle, D. Collen, J. Vermeylen, M. F. Hoylaerts, *Blood* 1999, 94, 2725.
- [51] G. C.G., S. R., C. S., *Cell Motil.* 1998, 40, 317.
- [52] D. Vestweber, *Atertio. Thromb. Vasc. Biol.* 2008, 28, 223.
- [53] S. D. Auerbach, L. Yang, F. W. Lusinskas, in *Adhesion Molecules: Function and Inhibition*, Springer, 2007, 99.
- [54] J. Fleischer, E. Soeth, N. Reiling, E. Grage - Griebenow, H. D. Flad, M. Ernst, *Immunology* 1996, 89, 592.
- [55] T. K. Hsiai, S. K. Cho, P. K. Wong, M. Ing, A. Salazar, A. Sevanian, M. Navab, L. L. Demer, C.-M. Ho, *The FASEB Journal* 2003, 17, 1648.
- [56] C. Dong, X. X. Lei, *J. Biomech.* 2000, 33, 35.
- [57] J. J. Campbell, J. Hedrick, A. Zlotnik, M. A. Siani, D. A. Thompson, E. C. Butcher, *Science* 1998, 279, 381.
- [58] S. L. Deshmane, S. Kremlev, S. Amini, B. E. Sawaya, *J. Interferon Cytokine Res.* 2009, 29, 313.
- [59] D. Loessner, C. Meinert, E. Kaemmerer, L. C. Martine, K. Yue, P. A. Levett, T. J. Klein, F. P. W. Melchels, A. Khademhosseini, D. W. Hutmacher, *Nat. Protocols* 2016, 11, 727.
- [60] K. Yue, X. Li, K. Schrobback, A. Sheikhi, N. Annabi, J. Leijten, W. Zhang, Y. S. Zhang, D. W. Hutmacher, T. J. Klein, *Biomaterials* 2017, 139, 163.
- [61] Y. Zhou, S. Yoshida, Y. Kubo, T. Yoshimura, Y. Kobayashi, T. Nakama, M. Yamaguchi, K. Ishikawa, Y. Oshima, T. Ishibashi, *Mol. Med. Report.* 2017, 15, 3949.
- [62] M. Jaguin, N. Houlbert, O. Fardel, V. Lecreur, *Cell. Immunol.* 2013, 281, 51.

- [63] A. a. M. A. Baqui, T. F. Meiller, J. J. Chon, B. F. Turng, W. A. Falkler Jr, *Oral Microbiol. Immunol.* 1998, 13, 173.
- [64] B.-H. Cha, S. R. Shin, J. Leijten, Y.-C. Li, S. Singh, J. C. Liu, N. Annabi, R. Abdi, M. R. Dokmeci, N. E. Vrana, A. M. Ghaemmaghami, A. Khademhosseini, *Adv. Healthcare Mater.* 2017, 6, 1700289.
- [65] H. M. Rostam, S. Singh, F. Salazar, P. Magennis, A. Hook, T. Singh, N. E. Vrana, M. R. Alexander, A. M. Ghaemmaghami, *Immunobiology* 2016, 221, 1237.
- [66] E. Mendoza-Coronel, E. Ortega, *Front. Immunol.* 2017, 8.
- [67] M. Genin, F. Clement, A. Fattaccioli, M. Raes, C. Michiels, *BMC Cancer* 2015, 15, 577.
- [68] S. An, S. Kim, Y. Huh, T. R. Lee, H.-K. Kim, K.-L. Park, H. C. Eun, *Contact Dermatitis* 2009, 60, 185.
- [69] B. H. Cha, S. R. Shin, J. Leijten, Y. C. Li, S. Singh, J. C. Liu, N. Annabi, R. Abdi, M. R. Dokmeci, N. E. Vrana, *Adv. Healthcare Mater.* 2017, 6, 1700289.
- [70] C. Dollinger, A. Ndreu - Halili, A. Uka, S. Singh, H. Sadam, T. Neuman, M. Rabineau, P. Lavallo, M. R. Dokmeci, A. Khademhosseini, *Advanced Biosystems* 2017, 1, 1700041.
- [71] E. Rieger, A. Dupret-Bories, L. Salou, M.-H. Metz-Boutigue, P. Layrolle, C. Debry, P. Lavallo, N. E. Vrana, *Nanoscale* 2015, 7, 9908.
- [72] S. Singh, D. Awuah, H. M. Rostam, R. D. Emes, N. K. Kandola, D. Onion, S. S. Htwe, B. Rajchagool, B.-H. Cha, D. Kim, *ACS Biomaterials Science & Engineering* 2017, 3, 969.
- [73] J. W. Nichol, S. T. Koshy, H. Bae, C. M. Hwang, S. Yamanlar, A. Khademhosseini, *Biomaterials* 2010, 31, 5536.
- [74] D. Loessner, C. Meinert, E. Kaemmerer, L. C. Martine, K. Yue, P. A. Levett, T. J. Klein, F. P. Melchels, A. Khademhosseini, D. W. Huttmacher, *Nat Protoc* 2016, 11, 727.
- [75] W. Liu, M. A. Heinrich, Y. Zhou, A. Akpek, N. Hu, X. Liu, X. Guan, Z. Zhong, X. Jin, A. Khademhosseini, Y. S. Zhang, *Adv. Healthcare Mater.* 2017, 6, 1601451.
- [76] N. Norouzi, H. C. Bhakta, W. H. Grover, *PLoS One* 2017, 12, e0180520.
- [77] F. Geissmann, S. Jung, D. R. Littman, *Immunity* 2003, 19, 71.
- [78] S. García-Nieto, R. K. Johal, K. M. Shakesheff, M. Emara, P.-J. Royer, D. Y. Chau, F. Shakib, A. M. Ghaemmaghami, *PLoS One* 2010, 5, e10123.
- [79] A. B. Zoladek, R. K. Johal, S. Garcia-Nieto, F. Pascut, K. M. Shakesheff, A. M. Ghaemmaghami, I. Notingher, *Analyst* 2010, 135, 3205.

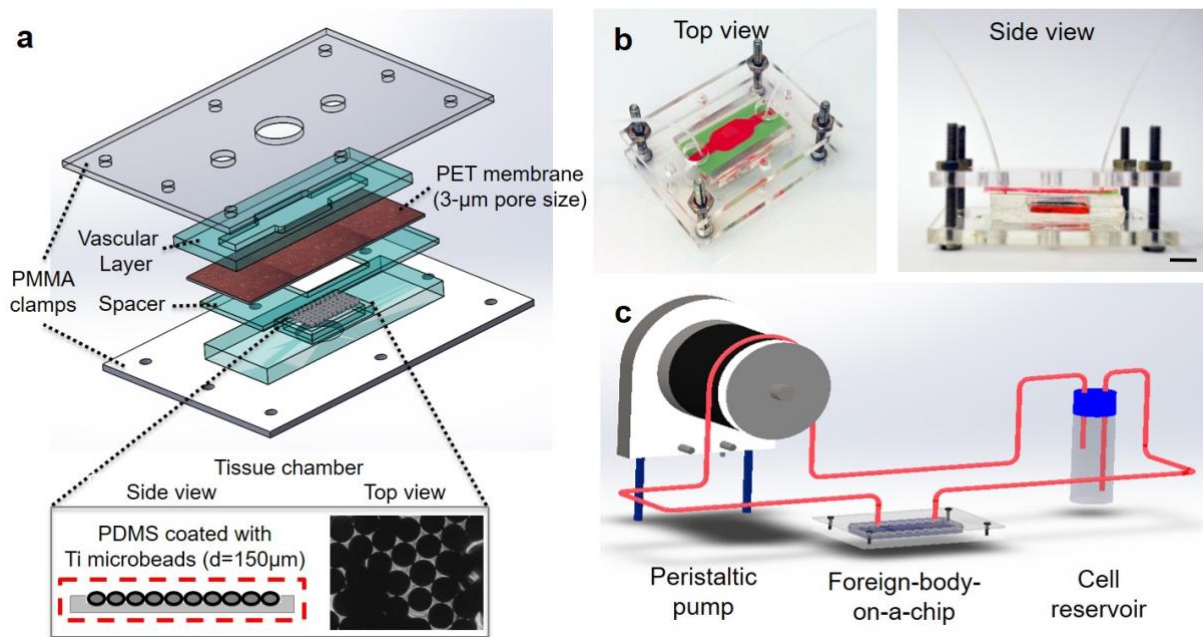


Fig. 1. Design of the FBROC device. A) Exploded schematic diagram showing the multi-layer structure of the bioreactor, where an endothelialized porous membrane is sandwiched in between a vascular channel on top and a tissue chamber at the bottom, the latter of which implant of Ti microbeads was placed. B) Perspective-view and side-view photographs showing the bioreactor in the multi-layer configuration. C) Schematic diagram showing the operation of the FBROC device, where immune cells are circulated from the top vascular channel of the bioreactor to probe their interactions with the Ti microbeads in the bottom tissue chamber through the endothelial barrier.

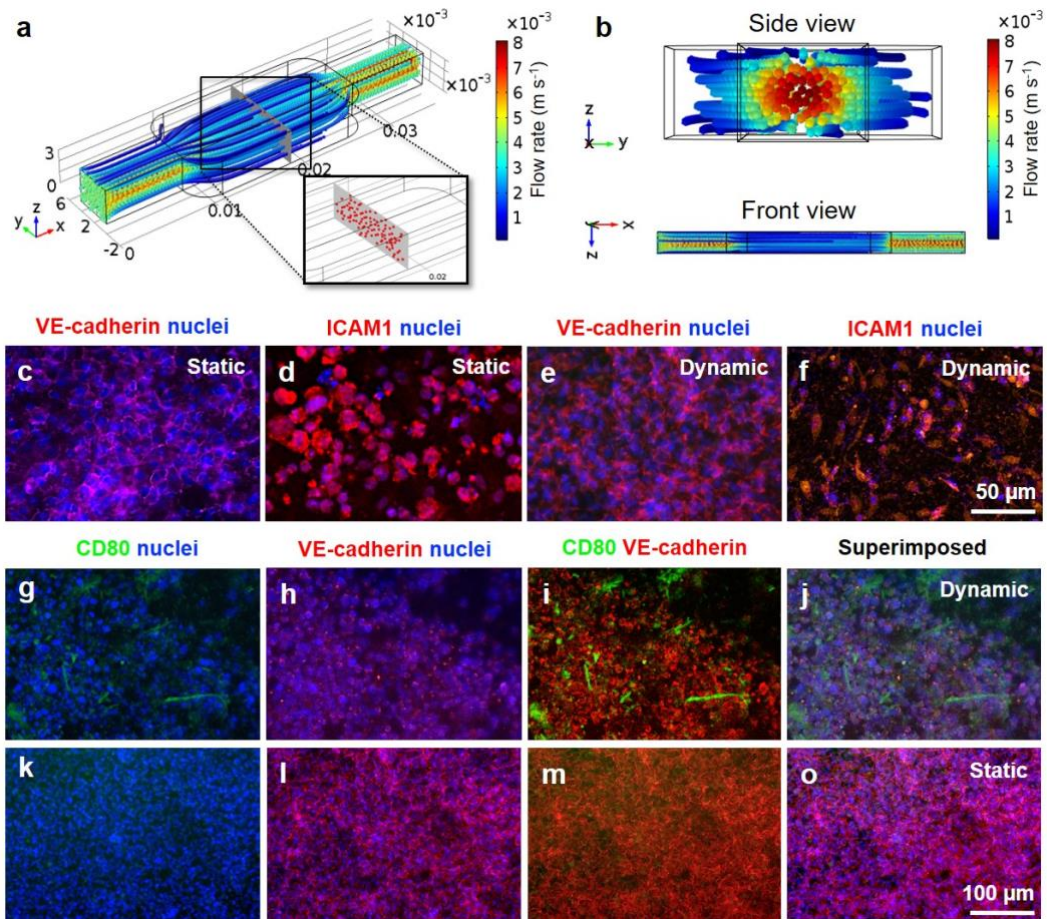


Fig. 2. Characterization of monocyte distribution, vascular barrier, and monocyte-endothelium interactions. A, B) Simulated distributions of the circulating immune cells in the top vascular channel of the bioreactor. C-F) Immunostaining of VE-cadherin and ICAM for confluent HUVECs cultured under (C, D) static and (E, F) dynamic conditions on the porous PET membrane. G-O) THP-1 monocyte interactions with the confluent endothelium under static and dynamic conditions.

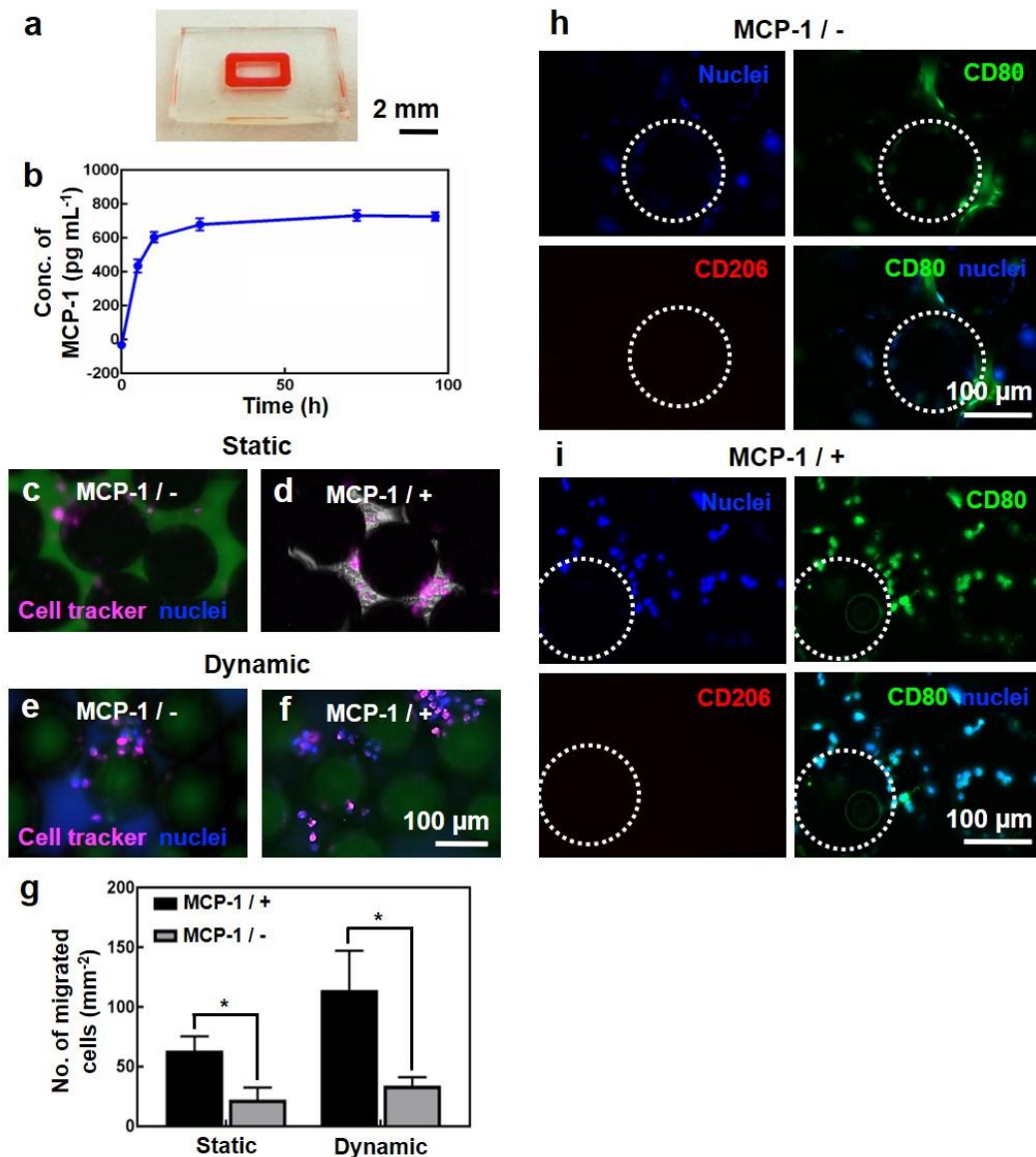


Fig. 3. FBR of THP-1 monocytes to the Ti microbeads. A) Photograph showing the GelMA hydrogel ring in the bottom tissue chamber for MCP-1 release. B) MCP-1 release over a 96-h period. (C-F) THP-1 monocyte trans-endothelial migration towards the bottom Ti microbeads under (C, D) static and (E, F) dynamic conditions, in the (C, E) absence and (D, F) presence of MCP-1. The cells were pre-labeled with cell tracker (pink) and post-labeled for nuclei (blue). (G) Quantifications of the number of THP-1 monocyte migration. H, I) CD80 (green)/CD206 (red) expressions of activated THP-1 monocytes on the Ti microbeads, in the (H) absence and (I) presence of MCP-1, under dynamic conditions. The nuclei were counterstained in blue. The white dotted circles indicate the Ti microbeads. * $p < 0.05$.

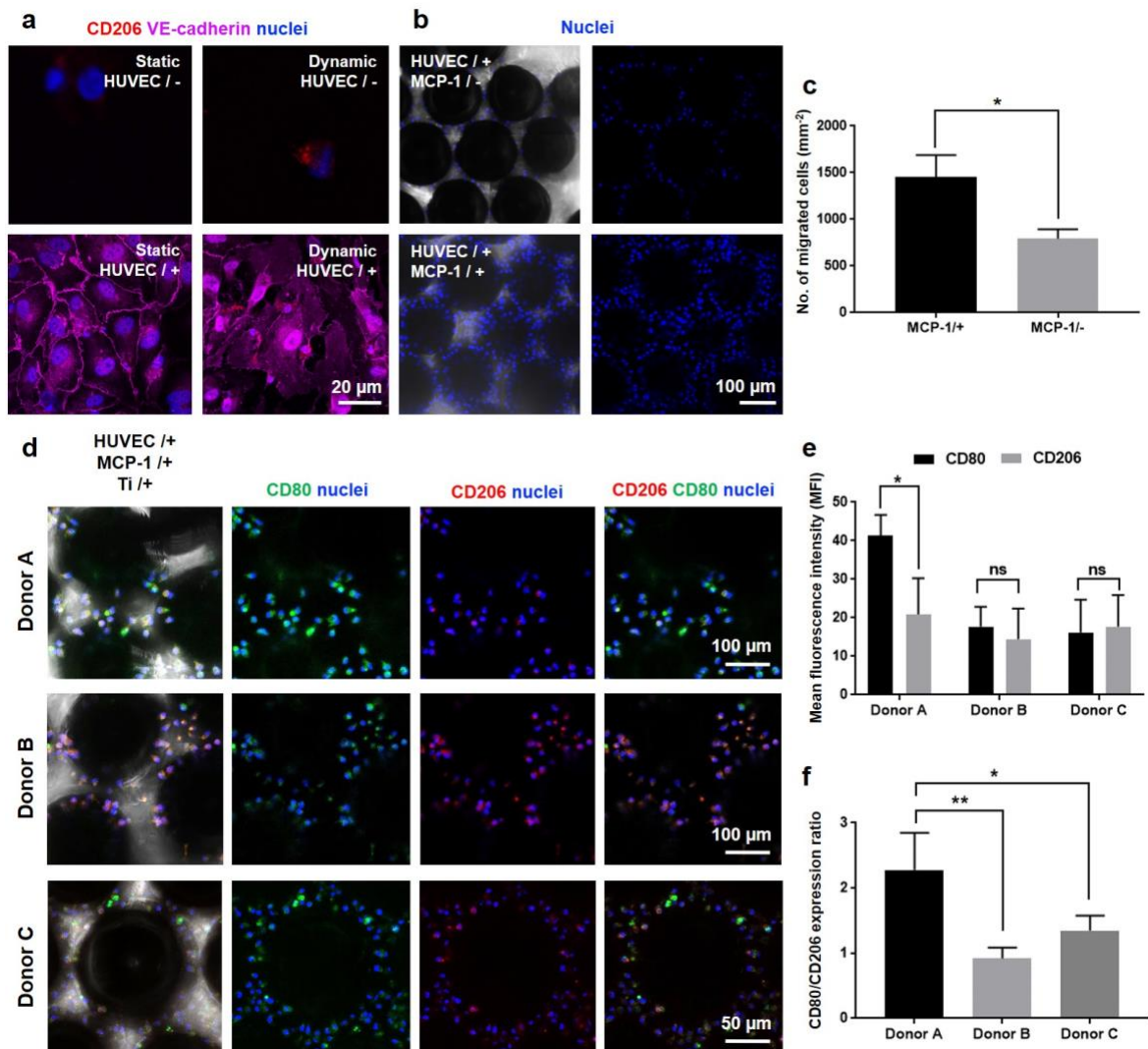


Fig. 4. Donor-specific FBR of patient PBMC-derived monocytes to the Ti microbeads. A) Monocyte/PET membrane interactions in the absence or presence of HUVECs under static or dynamic conditions. B) Trans-endothelial migration of monocytes onto Ti microbeads in the bottom tissue chamber in the absence or presence of MCP-1 under dynamic conditions. C) Quantification of trans-endothelial migration of monocytes onto Ti microbeads in the bottom tissue chamber in the absence / or presence of MCP-1. d) CD206/CD80 expressions of activated monocytes from three different human donors on Ti microbeads in the presence of MCP-1 under dynamic conditions. e) Quantifications of CD206 and CD80 expressions of activated monocytes on the Ti microbeads in the presence of MCP-1 under dynamic conditions for monocytes derived from three different human donors. f) Quantifications of CD206/CD80 expression ratios of activated monocytes on the Ti microbeads in the presence of MCP-1 under

dynamic conditions for monocytes derived from three different human donors. * $p < 0.05$, **
 $p < 0.01$.

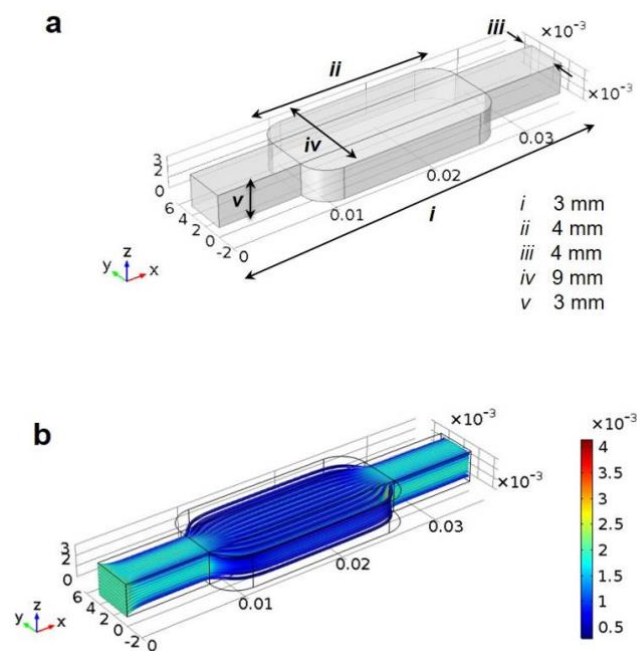


Fig. S1. Characterizations of the bioreactor. A) Dimensions of the top vascular channel of the bioreactor. B) Flow velocity profiles in the vascular chamber of the bioreactor.

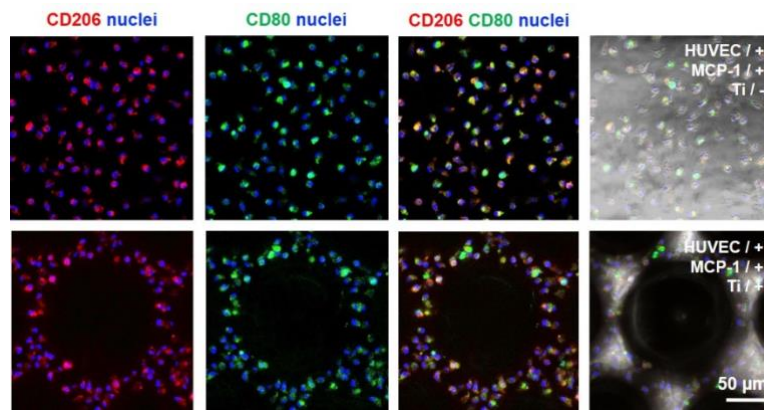


Fig. S2. FBR of patient-derived monocytes to Ti microbeads. CD206/CD80 expressions of activated monocytes at the bottom tissue chamber, in the absence or presence of Ti microbeads, under dynamic conditions with the release of MCP-1.